

Chapman University Chapman University Digital Commons

Mathematics, Physics, and Computer Science
Faculty Articles and Research

Science and Technology Faculty Articles and
Research

3-28-2019

Using Multi-indices Approach to Quantify Mangrove Changes Over the Western Arabian Gulf along Saudi Arabia Coast

Wenzhao Li
Chapman University

Hesham el-Askary
Chapman University, elaskary@chapman.edu

Mohamed A. Qurban
King Fahd University of Petroleum and Minerals

Jingjing Li
California State University, Los Angeles

K. P. ManiKandan
King Fahd University of Petroleum and Minerals

Follow this and additional works at: https://digitalcommons.chapman.edu/scs_articles

 Part of the [Environmental Health and Protection Commons](#), [Environmental Indicators and Impact Assessment Commons](#), [Environmental Monitoring Commons](#), [Forest Biology Commons](#), [Other Earth Sciences Commons](#), [Other Environmental Sciences Commons](#), [Other Forestry and Forest Sciences Commons](#), and the [Sustainability Commons](#)

Recommended Citation

Li, W., El-Askary, H., Qurban, M.A., Li, J., ManiKandan, M.P., Piechota, T., 2019. Using multi-indices approach to quantify mangrove changes over the Western Arabian Gulf along Saudi Arabia coast. *Ecological Indicators* 102, 734-745. <https://doi.org/10.1016/j.ecolind.2019.03.047>

This Article is brought to you for free and open access by the Science and Technology Faculty Articles and Research at Chapman University Digital Commons. It has been accepted for inclusion in Mathematics, Physics, and Computer Science Faculty Articles and Research by an authorized administrator of Chapman University Digital Commons. For more information, please contact laughtin@chapman.edu.

Using Multi-indices Approach to Quantify Mangrove Changes Over the Western Arabian Gulf along Saudi Arabia Coast

Comments

NOTICE: this is the author's version of a work that was accepted for publication in *Ecological Indicators*. Changes resulting from the publishing process, such as peer review, editing, corrections, structural formatting, and other quality control mechanisms may not be reflected in this document. Changes may have been made to this work since it was submitted for publication. A definitive version was subsequently published in *Ecological Indicators*, volume 102, in 2019. DOI: [10.1016/j.ecolind.2019.03.047](https://doi.org/10.1016/j.ecolind.2019.03.047)

The Creative Commons license below applies only to this version of the article.

Creative Commons License



This work is licensed under a [Creative Commons Attribution-Noncommercial-No Derivative Works 4.0 License](https://creativecommons.org/licenses/by-nc-nd/4.0/).

Copyright

Elsevier

Authors

Wenzhao Li, Hesham el-Askary, Mohamed A. Qurban, Jingjing Li, K. P. ManiKandan, and Thomas Piechota

1 **Using Multi-indices Approach to Quantify Mangrove Changes over the**
2 **Western Arabian Gulf along Saudi Arabia Coast**

3 Wenzhao Li ^a, Hesham El-Askary ^{b,c,d,*}, Mohamed A. Qurban ^{e,f}, Jingjing Li ^g, K. P.
4 ManiKandan ^e, Thomas Piechota ^c

5
6 ^a Computational and Data Sciences Graduate Program, Schmid College of Science and
7 Technology, Chapman University, Orange, California 92866, USA

8 ^b Center of Excellence in Earth Systems Modeling & Observations, Chapman University,
9 Orange, 92866, California, USA

10 ^c Schmid College of Science and Technology, Chapman University, Orange, 92866,
11 California, USA

12 ^d Department of Environmental Sciences, Faculty of Science, Alexandria University,
13 Moharem Bek, Alexandria, 21522, Egypt

14 ^e Center for Environment and Water, The Research Institute, King Fahd University of
15 Petroleum and Minerals (KFUPM), Dhahran, 31261, Kingdom of Saudi Arabia

16 ^f Geosciences Department, the college of Petroleum Engineering & Geosciences, King
17 Fahd University of Petroleum and Minerals (KFUPM), Dhahran, 31261, Kingdom of
18 Saudi Arabia

19 ^g Department of Geosciences and Environment, California State University Los Angeles,
20 CA 90032, USA

21
22 Contact Hesham El-Askary; Tel.: +1 714 289 2053; E-mail: elaskary@chapman.edu;
23 Schmid College of Science and Technology, Chapman University, 1 University Drive,
24 Orange CA 92866, USA

25
26 **Abstract**

27 Mangroves habitat present an important resource for large coastal communities
28 benefiting from activities such as fisheries, forest products and clean water as well as

29 protection against coastal erosion and climate related extreme events. Yet they are
30 increasingly threatened by natural pressure and anthropogenic activities. We observed an
31 inaccurate distribution of mangroves over the Western Arabian Gulf (WAG) which is a
32 vital habitat and resource for the local ecosystem, according to the United States
33 Geological Survey (USGS) mangrove database through spectral analysis. Change
34 detection analysis is conducted on mangrove forests along the Saudi Arabian coast of the
35 WAG for the years 2000, 2010 and 2018 using Landsat 7 & 8 data. Three supervised
36 classification methodologies are employed for mangrove mapping, including Supported
37 Vector Machine (SVM), Decision Tree (DT), referred to as Classification and Regression
38 Trees (CART) and Random Forest (RF). CART's accuracy was recorded to be >95%
39 while other classifiers were >90%. The CART supervised learning classifier, mapping
40 mangroves' distribution and biomass using Google Earth Engine (GEE) online platform,
41 indicates an overall increase in the northern Tarut Bay and Tarut Island, by 0.21 km² from
42 2000 to 2010 and by 1.4 km² from 2010 to 2018. The increase might be due to mitigation
43 strategies such as mangrove breeding and plantation. It can be challenging to detect
44 changes in certain regions due to the inadequate resolution of Landsat where submerged
45 mangroves can be confused with salt marshes and macro algae. We employed a new
46 method to identify and analyze submerged mangrove forests distribution via a submerged
47 mangrove recognition index (SMRI) and normalized difference vegetation index (NDVI)
48 in Abu Ali Island. Our results show the robustness of SMRI as an effective indicator to
49 detect submerged mangroves in both high and medium spatial resolution satellite images.
50 NDVI values differentiated submerged mangroves from tidal flats between Landsat 7 &
51 8 as well as during conditions of low and high tides. High resolution WorldView-2 image
52 showed agreement of mangroves distribution with the SMRI and NDVI results.

53

54 **Keywords**

55 Mangrove; Arabian Gulf; Google Earth Engine; Landsat; Ecological Indices, Change
56 detection; Classification Methodologies

57

58 **Abbreviations**

59 SMRI, submerged mangrove recognition index; NDVI, Normalized Difference
60 Vegetation Index; GEE, Google Earth Engine; WAG, Western Arabian Gulf.

61

62 **1. Introduction**

63 Mangrove forests are present in the intertidal zone, located within small groups of
64 trees and shrubs in the harsh interface between sea and land. They are distributed largely
65 in the tropical and subtropical areas between 30°N and 30°S latitude. As a habitat to rich
66 and biologically complex species, they are one of the most productive ecosystems in the
67 world (Donato et al., 2011), providing considerable services to human communities with
68 ecological and economic values to protect shoreline from storms, erosion, and
69 sedimentation (Moore et al., 2015), as well as providing nutrients for algae blooms (Li et
70 al., 2017; Li et al., 2018). The protective role of mangrove forests was also recognized
71 during Asian Tsunami of 2004 and other natural disasters such as hurricanes (Danielsen,
72 2005; Kathiresan and Rajendran, 2005). The analysis of the economic values of the
73 mangrove forests is necessary for integrated land use planning and environmental
74 decision-making (Vo et al., 2012). A Mangrove Quality Index (MQI), ranking 1(worst)
75 to 5 (excellent), was developed to evaluate the overall mangrove health status of
76 mangrove ecosystems in Matang, Malaysia (Faridah-Hanum et al., 2019).

77 In addition, mangrove forests, acting as significant carbon sinks, play an important
78 role in climate change (Donato et al., 2011). However, mangroves are threatened due to

79 both anthropogenic and natural stressors. For instance, over the western Arabian Gulf,
80 increased soil contaminations of heavy metals was found in the mangrove habitats (Al-
81 Kahtany et al., 2018; Almahasheer, 2019). One third of their forests has been lost in the
82 past half century (Alongi, 2002). It is estimated that 35% of the mangrove forests were
83 lost during 1980 to 2005 (Millennium Ecosystem Assessment, 2005) in a much faster
84 declining rate than coral reefs and inland tropical forests (Duke et al., 2007). Mangrove
85 habitat land use change is used as an indicator for environmental quality, for instance,
86 such a change can affect soil microbial biomass (Dinesh and Ghoshal Chaudhuri, 2013),
87 as well as intertidal fish communities (Ellis and Bell, 2013). If no actions are taken to
88 protect the mangrove ecosystem, 30%-40% of coastal wetlands and 100% of mangrove
89 forest could lose their functionalities in the next 100 years with the present declining rate
90 (Shapiro et al., 2015).

91 Mangrove forests cover around 152,000 km² in 123 countries and territories in the
92 tropics and subtropics of the world (Spalding et al., 2010), among which Middle East
93 region has 624 km², about 0.4% of global coverage. Arabian Gulf, one of the most
94 important inland sea at this region, is little known about its coverage and distribution of
95 mangrove forests. The Arabian Gulf is a shallow basin of an average depth of 35m,
96 extending approximately 24° - 30°N and 48° - 56°E (Al-Muzaini and Jacob, 1996). Its
97 coastlines, which is the most arid in the world, were formed in the past 3000 – 6000 years
98 (Burt, 2014). The water temperature vary from around 12°C - 35°C (Price et al., 1993),
99 and the surface temperature in intertidal zones can exceed 50°C in the summer (Burt,
100 2014). The salinity in the Arabian Gulf is as high as 43 psu and may even reach 70-80
101 psu in tidal pools and lagoons. This is due to the high-latitude geographical location, high
102 evaporation rates, as well as relative shallowness. In such an extreme environment, most
103 of the marine species in the Arabian Gulf reach their tolerance limits (Price et al., 1993).

104 Mangroves, however, are able to survive in this region because they tolerate the high
105 salinity at early stages of development (Naser and Hoad, 2011). One type of mangroves,
106 *Avicennia marina*, can be sparsely found at the southern shores, confined to sheltered
107 coastal areas along the coastlines of Saudi Arabia, Arab Emirates and Qatar (Burt, 2014).
108 Despite the low volume, low diversity and intermittent occurrence of mangroves, the
109 presence is of significant ecological importance in this region. Mangroves are among the
110 only trees in the desert landscape, offering food for livestock and other wild animals.
111 They support a variety of essential species of birds, fish, shrimps and turtles, contributing
112 substantially to the coastal productivity (Al-Maslamani et al., 2013). It has been reported
113 that Tarut Bay alone has lost a significant 55% mangrove forests (mostly in the south part)
114 from 1972 till 2011 (Almahasheer et al., 2013). This is attributed to human and
115 environmental pressures such as pollutants, land reclamation and urban encroachment.
116 On the other hand a regional research of decadal changes of the Red Sea mangrove forest
117 showed a slight increase of its coverage (Almahasheer et al., 2016). Fortunately, the
118 mangrove forests has been in a recovery process with small increase by plantation
119 activities by both government (i.e., the Ministry of Agriculture) and industry (Saudi-
120 Aramco 2016) in Saudi Arabia. As early as 1970s, vegetation indices had been used for
121 quantitative measurement of vegetation conditions (Rouse et al., 1973; Gitelson et al.,
122 1996; Ahamed et al., 2011). High spatial resolution remote sensing imagery could
123 generate various vegetation indices, such as Normalized Difference Vegetation Index
124 (NDVI, NDVI2), Normalized Difference Red Edge index (NDRE, NDRE2), Green
125 Normalized Difference Vegetation Index (GNDVI) and Chlorophyll Vegetation Index
126 (CVI), which have been widely investigated to mangrove and other species, such as
127 mangrove canopy chlorophyll concentration (Heenkenda et al., 2014, 2015, Vincini et al.,
128 2007, 2008), feedstock biomass production (Ahamed et al., 2011), and low and high

129 density mangrove estimation (Mutanga et al., 2012; Al-Ali et al. 2015; Almahasheer et
130 al. 2013, 2016).

131 Mangroves have very distinct spectral features in remote sensing data, especially in
132 the spectral ranges corresponding to the visible red, near-infrared, and mid-infrared,
133 making it easier to classify than other land cover types. The best combination of spectral
134 bands to detect mangroves are Landsat 7 bands 3 (0.63–0.69 μm), 4 (0.77–0.90 μm), 5
135 (1.55–1.75 μm), and 7 (2.09–2.35 μm) (Giri, 2016). Therefore, indices like the Normalized
136 Difference Vegetation Index (NDVI) are useful in identification it has been employed for
137 other applications (Kim et al., 2014; Whitney et al., 2018). Recent advancement in
138 computing and information technology, image-processing methodologies, as well as the
139 availability of remote sensing data, have provided an opportunity to monitor mangroves
140 at regional and global scales on a consistent and regular basis. Meanwhile, there has been
141 an increase in high-performance cloud computing platforms, such as the NASA Earth
142 Exchange (NEX), Amazon Web Service (AWS), and Google Earth Engine (GEE). The
143 advantages of cloud computing include the parallel computing, offering nearly unlimited
144 computer processing capabilities, as well as free access to a large volume of satellite
145 remote sensing data stored in the remote cloud drives. This eliminates the need for large
146 external hard disk storage and facilitates easy data access. For example, GEE provides
147 preprocessed Sentinel data (2014 - present), Landsat data (1982-present), as well as
148 advanced classification machine learning algorithms accessible through JavaScript and
149 Python programs (Giri et al., 2015). One research project utilized GEE to analyze the
150 changes of mangrove forests over 30 years in Thailand (Pimple et al., 2018). It is
151 noteworthy that this Thailand mangrove study didn't use the Landsat 7 data after 2003
152 and had a missing scene in the year of 2012. This is because Landsat 7 Enhanced
153 Thematic Mapper (ETM) sensor had a failure of the Scan Line Corrector (SLC) on 31

154 May 2003. Since that time all Landsat ETM data has wedge-shaped gaps on both sides of
155 each scene, resulting in approximately 22% of data loss.

156 Mangrove forests mapping methods are usually based on a single-day imagery
157 analysis, which can suffer from low or high tides. Such analysis can suffer by not taking
158 the tide levels into consideration given that mangrove forests are periodically submerged
159 by tides. This can impose a problem of over or under estimation in mangrove mapping
160 when the images are observed during high-tide periods. Since mangroves grow along
161 often-narrow extent along coastlines, detailed mangrove ecosystem characterization
162 becomes difficult with moderate-resolution (30 m) satellite data and there is a need for
163 high-resolution imagery to gain more accurate mapping results at different tide levels
164 (Green et al., 1998). A recent study proposed a new method to identify submerged
165 mangrove forests via a submerged mangrove recognition index (SMRI) using high-
166 resolution satellites' images, which considered different spectral signatures of mangroves
167 under both low and high tide levels (Xia et al., 2018). However, due to naturally and/or
168 human factors, mangrove communities along the Arabian Gulf coastlines covering more
169 than 165 km² are predominantly separated from each other (Almahasheer, 2018). This
170 fragmentation brings massive cost to study mangrove at a regional scale with only using
171 high resolution remote sensing images. For example, SA has a 700 km long coastline in
172 WAG (Bird, 2010). This will cost around \$26,600 for getting entire coastline using
173 WorldView-2 images with 8-bands for one time period (calculated from price listed in
174 www.landinfo.com: \$19/km² with 2 km minimum order width). The mangrove change
175 detection study of two periods will cost double the price. Therefore, there is a need to
176 improve mangrove detection methods through free accessible medium-resolution satellite
177 imagery (such as Landsat 7/8). Here we employed high resolution images for selected
178 regions for validation purposes.

179 We present a multi-indices based approach, using NDVI and SMRI, for long term
180 mapping of mangrove forests in the WAG region along the Saudi Arabia coast. In this
181 study, we evaluate the accuracy of three existing mangrove forests datasets and for the
182 first time, incorporated SMRI as a new assessment for detecting submerged mangrove at
183 different tide levels over the WAG region using Landsat medium-resolution remote
184 sensing images.

185

186 **2. Materials and methods**

187 *2.1 Data*

188 Three mangrove datasets were used in this research: 1) USGS Global Mangrove
189 Forest Distribution of year 2000 (Giri et al., 2011). This dataset was generated using
190 Landsat satellite images of more than 1,000 scenes obtained from the USGS Earth
191 Resources Observation and Science Center (EROS). Mangroves were classified using
192 hybrid supervised and unsupervised digital image classification techniques. 2) World
193 Atlas of Mangroves. This dataset shows the global distribution of mangroves, and was
194 produced as a joint initiative of the Food and Agriculture Organization of the United
195 Nations (FAO), the International Tropical Timber Organization (ITTO), International
196 Society for Mangrove Ecosystems (ISME), UN Environment World Conservation
197 Monitoring Centre (UNEP-WCMC) (Spalding et al., 2010), United Nations Educational,
198 Scientific and Cultural Organization's Man and the Biosphere Programme (UNESCO-
199 MAB), United Nations University Institute for Water, Environment and Health (UNU-
200 INWEH), and The Nature Conservancy (TNC). 3) Global Distribution of Modelled
201 Mangrove Biomass (2014) (Hutchison et al., 2014). This dataset was developed by the
202 Department of Zoology in University of Cambridge, with the support from The Nature
203 Conservancy. It shows the global patterns of above-ground biomass of mangrove forests

204 based on a review of 95 field studies on carbon storage and fluxes in mangroves world-
205 wide.

206 Two kinds of remote sensing images are used here: 1) WorldView-2 image.
207 WorldView-2 is a high-resolution satellite launched on October 8, 2009 from Vandenberg
208 Air Force Base, CA. WorldView-2 collects 46-centimeter (cm) panchromatic and 1.85-
209 meter (m) multispectral imagery. In this research, we obtained the image of four
210 traditional bands (i.e. blue, green, red and NIR) over the Abu Ali Island during
211 September, 2017 to study for the submerged mangrove detection. 2) Landsat 5, Landsat
212 7, and Landsat 8 Surface Reflectance Tier 1 dataset from the Landsat 5 TM, Landsat 7
213 ETM+ sensor and Landsat 8 OLI/TIRS sensors. These images contain 4 visible and near-
214 infrared (VNIR) bands of 30m resolution for Landsat 7 (5 VNIR bands for Landsat 8), 2
215 short-wave infrared (SWIR) bands of 30m resolution processed to orthorectified surface
216 reflectance, and one thermal infrared (TIR) band of resampled 30m resolution for Landsat
217 5/7 (2 thermal bands for Landsat 8) processed to orthorectified brightness temperature.
218 The surface reflectance dataset was provided from GEE. They have been atmospherically
219 corrected using The Landsat Ecosystem Disturbance Adaptive Processing System
220 (LEDAPS), and include a per-pixel saturation mask and a cloud, shadow, water and snow
221 mask produced using C Function of Mask (CFMASK). In this study, we utilized Landsat
222 5 image of 1985, Landsat 7 images of 2000, 2010 and 2018, and Landsat 8 images of
223 2018 for the aforementioned three mangrove datasets for inter comparison. Landsat 7 and
224 8 images were also used for detecting the mangrove changes between 2000, 2010, and
225 2018. Moreover, we obtained and processed Landsat 7 and Landsat 8 images of 2017 to
226 quantify the submerged mangrove in Abu Ali Island based on tidal data. The tidal data
227 was accessed from the harmonic model by WorldTides™ (<https://www.worldtides.info>)
228 that uses a number of public and licensed sources for tidal predictions as well as land-

229 based station observations from tide gauges and satellite observations when available for
230 the maximum accuracy. Since tides are caused by the gravitational pull on water from the
231 sun, moon, and other planets, hence the gravitational pulls' frequencies are well known,
232 thus harmonic analysis models are employed here for future water levels prediction based
233 on past observations.

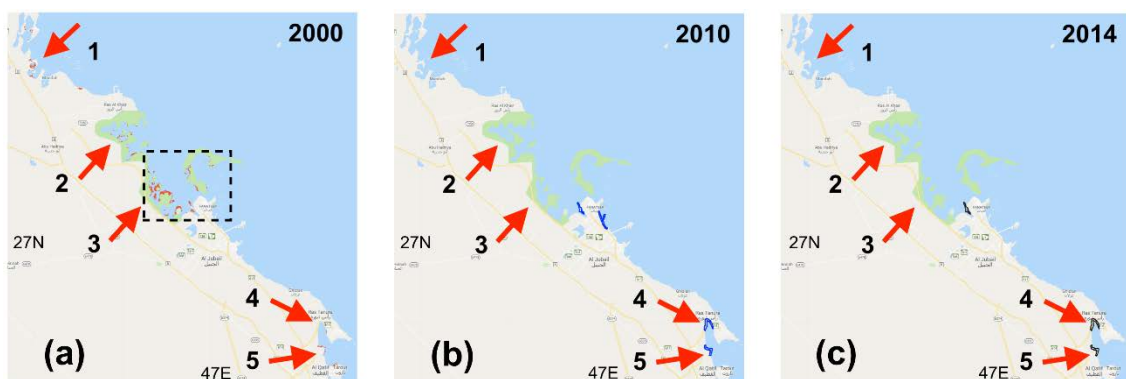
234

235 *2.2 Study region*

236 Fig.1 shows mangrove distribution for the years 2000, 2010 and 2014, respectively,
237 using the three existing mangrove datasets over the WAG. The 2000 image from USGS
238 Global Mangrove Forest Distribution is accessed through GEE searching tool, and 2010
239 image from World Atlas of Mangroves and 2014 image from Mangrove Forest Biomass
240 are converted into GeoTIFF format files, then imported into GEE. Along the coast of
241 Saudi Arabia, five regions are studied based on the mangroves' distribution: 1. Manifah,
242 2. Al-Khair, 3. Jubail, 4. North Tarut Bay, and 5. North Middle Tarut Bay, all marked by
243 correspondent numbers in the Fig.1. Fig.1 shows obvious differences among the three
244 datasets, for instance, mangroves in region 1 (Manifah) and region 2 (Al-Khair) can be
245 found in 2000 (pointed at by the red arrow), but disappeared in 2010 and 2014.
246 Mangroves of region 3 (Jubail) are observed in all three years, with the highest coverage
247 in 2000 highlighted in black squared area, whereas in 2010 and 2014 the mangrove only
248 be marked in the Gurmah Island (at location 3 in green color 2010 and red color 2014).

249 On the north side of region 4 (North Tarut Bay), both the 2010 (Fig. 1b) and 2014
250 (Fig. 1c) are marked with a mangrove distribution (pointed by a red arrow) near Ras
251 Tanura, but not much appearing in the 2000 data (Fig. 1a). In addition, mangroves are
252 distributed in region 5 (North Middle Tarut Bay) in the 2010 data (pointed by a red arrow
253 in Fig. 1b) and 2014 (Fig. 1c), while they do not appear that much in 2000 (Fig. 1a).

254 Therefore, it is clear that large discrepancies were identified among these three years
255 datasets. This could be explained either due to a massive decline and disappearance of
256 mangroves in 2000 in regions 1&2&3 after 2010 or a misclassification of the mangrove
257 dataset by USGS accounting for other species as mangroves. Therefore, accurate
258 assessment and validation work is highly needed to avoid misleading datasets, especially
259 if it were to be used to build models for future mangrove change detection researches and
260 for stakeholders and decision makers. In this study, we conducted a spectral analysis over
261 the commonly recognized mangrove areas (in regions 3, 4 and 5), and from uncertain
262 mangrove areas (region 3). The unique spectral signatures from mangrove habitats could
263 help accurately decide on the consistency of distribution for mangrove habitats across the
264 different data sets and at different locations.



265
266 Figure 1. Mangrove distribution in WAG for regions 1:Manifah, 2:Al-Khair, 3:Jubail, 4:North Tarut Bay,
267 5:North Middle Tarut Bay using (a) USGS Global Mangrove Forest Distribution of year 2000 (red color)
268 (b) World Atlas of Mangroves of the year 2010 (blue color) (c) Mangrove Forest Biomass of the year 2014
269 (black color). The red arrows point to the mangroves, and black box highlights the massive mangrove
270 coverage of USGS data.

271

272 2.3 Methodology

273 2.3.1 Classification methods

274 The workflow of generation and validation of mangrove classification model along
275 with the procedures of classifying mangrove forests follow the workflow of the change

276 detection analysis of coral reef habitat using Landsat data in the Red Sea (Hurghada,
277 Egypt) (El-Askary et al., 2014). The Landsat 7&8 images of the year 2018 are used to
278 generate different mangrove detection models, including Supported Vector Machine
279 (SVM), Decision Tree (DT), referred to as Classification and Regression Trees (CART)
280 and Random Forest (RF). The results of these models are evaluated by the accuracy
281 (generated from confusion matrices), and by comparing with high-resolution image from
282 Google Earth. Then the most effective models are selected to classify the mangrove
283 distribution for the areas of interest among the year of 2000, 2010, and 2018 using
284 Landsat 7&8 images. It is noteworthy that Landsat 5 did not provide image after August
285 1st 2002 in these regions. Alternatively, Landsat 7 images during the year 2010 were
286 processed with GEE built-in mosaicking method to guarantee ideal results.

287 *2.3.1.1 CART*

288 CART, a supervised classification mining method, is used here to construct a
289 decision binary tree structure through iterative analysis based on the training dataset that
290 consists of features (i.e. spectral signatures) and target variables (i.e. mangrove or other
291 classes) (Breiman, 1998). It has been widely used in land use analysis and change
292 detection (Rick L. Lawrence and Andrea Wright, 2001), wetlands and mangrove
293 distribution classification (Pantaleoni et al., 2009; Zhao et al., 2014). In this research, we
294 used the maximum tree depth which controls the maximum number of allowed levels
295 below the root node to construct the decision tree. Normally, the larger the maximum
296 tree depth value, the more complex the decision tree and the higher the classification
297 accuracy. Through multiple trials and the 10-fold cross validation, a maximum tree depth
298 value of ten was selected for the CART classification.

299 *2.3.1.2 SVM*

300 The SVM machine learning algorithm, a well-adapted technique for solving non-
301 linear, high dimensional space classifications, is used here as it showed a good
302 performance in mangrove satellite sensing (Heenkenda et al., 2014; Heumann, 2011;
303 Kanniah et al., 2015; Wang et al., 2018). It was found that SVM has better performance
304 than maximum likelihood and artificial neural network classifiers using Landsat TM
305 image (Pal and Mather, 2005). Moreover, SVM outperforms discriminate analysis and
306 decision-tree algorithms for airborne sensor data (Foody and Mathur, 2006). SVM
307 uniqueness from other traditional classification approaches stems from its ability to create
308 a hyperplane through n-dimensional spectral-space. This plane separates classes
309 (mangroves versus others) based on a user defined kernel function (linear in our case) and
310 parameters that are optimized using machine-learning to maximize the margin from the
311 closest point to the hyperplane.

312 2.3.1.3 RF

313 RF is a relatively new technique for mangrove species mapping, though it has been
314 widely applied in landscape (Duro et al., 2012; Li et al., 2016) and plant species (Le
315 Louarn et al., 2017; Ng et al., 2017) classification with different sensors in recent years.
316 The RF algorithm is an ensemble algorithm for supervised classification based on CART.
317 However, by combining the characteristics of CART together with further bootstrap
318 aggregating, and random feature selecting, independent predictions can be established
319 and therefore improve accuracies. For the RF algorithm, the tuning parameters mainly
320 included “number of features”. This controls the size of a randomly selected subset of
321 features at each split in the tree building process, which could have sensitive impact on
322 classification (Duro et al., 2012). The other tuning parameter also includes the maximum
323 number of trees (Su et al., 2017). In this research, the maximum level of trees used was
324 five above which the accuracy did not change much.

325 2.3.2 Submerged Mangrove Recognition Index (SMRI)

326 Most previous change detection research of mangrove forests are based on remote
327 sensing images captured at different dates, not considering the impacts of tide level
328 changes (Collins et al., 2017; Li et al., 2013; Rogers et al., 2017; Xia et al., 2018).
329 However, mangrove forests are distributed near the land–sea interface, such as shorelines
330 and in elongated or fragmented patches, especially in the WAG. These mangroves
331 periodically receive inundation of sea water, where the fluctuating water underneath the
332 canopy dramatically changes the spectral signatures as observed using satellite images.
333 Therefore, it is difficult to retrieve accurate mangrove information using the methods
334 based on single-day remote sensing imagery comparison of vegetation indices (i.e.
335 NDVI). Recently, Xia et al. (2018) proposed a submerged mangrove recognition index
336 (SMRI) by using high-resolution GF-1 images in both low and high tides, to describe the
337 unique spectral signature of submerged mangroves and to distinguish mangroves forests
338 submerged by different tide levels. The detailed form of the SMRI index is based on a
339 combination of NDVI (Rouse et al., 1973) and near-infrared bands, shown below:

$$340 \text{ SMRI} = (NDVI_l - NDVI_h) \times \frac{NIR_l - NIR_h}{NIR_h} \quad [1]$$

$$341 NDVI_l = \frac{NIR_l - R_l}{NIR_l + R_l} \quad [2]$$

$$342 NDVI_h = \frac{NIR_h - R_h}{NIR_h + R_h} \quad [3]$$

340 where $NDVI_l$ and $NDVI_h$ are the NDVI values at low tide and high tide, respectively.
341 NIR_l and NIR_h are the reflectance values of the near-infrared band at low and high tide,
342 respectively. R_l and R_h are the reflectance values of the red band at low and high tide,
343 respectively. In this research, we apply this index for detecting the submerged mangrove
344 forests with Landsat medium-resolution imagery.

345 We also conducted studies to look at the effects of tide levels on the mangrove
346 classification. WorldView-2 image was utilized to provide training data and validation
347 for unsupervised classification cluster of mangrove in Abu Ali Island during the limited
348 time period of September 2017. Landsat 7&8 images were used to implement the
349 unsupervised classification method to explore the attributes of submerged mangroves for
350 the same time period over the same region. All of the images were preprocessed, subset
351 for coastal areas only and not including terrestrial vegetation and masked for marine
352 habitats only and excluding water and land. We also applied the NDVI and SMRI, a new
353 indicator to improve the submerged mangrove detection and to detect tidal impacts. It is
354 noteworthy that all the Landsat and WorldView-2 images are visualized with false color
355 configurations (R: near infrared band, G: red band, B: green band) to highlight the
356 vegetation as red areas. Supervised classification models using three algorithms (CART,
357 SVM and Random Forest) are implemented here to distinguish mangrove habitats from
358 others.

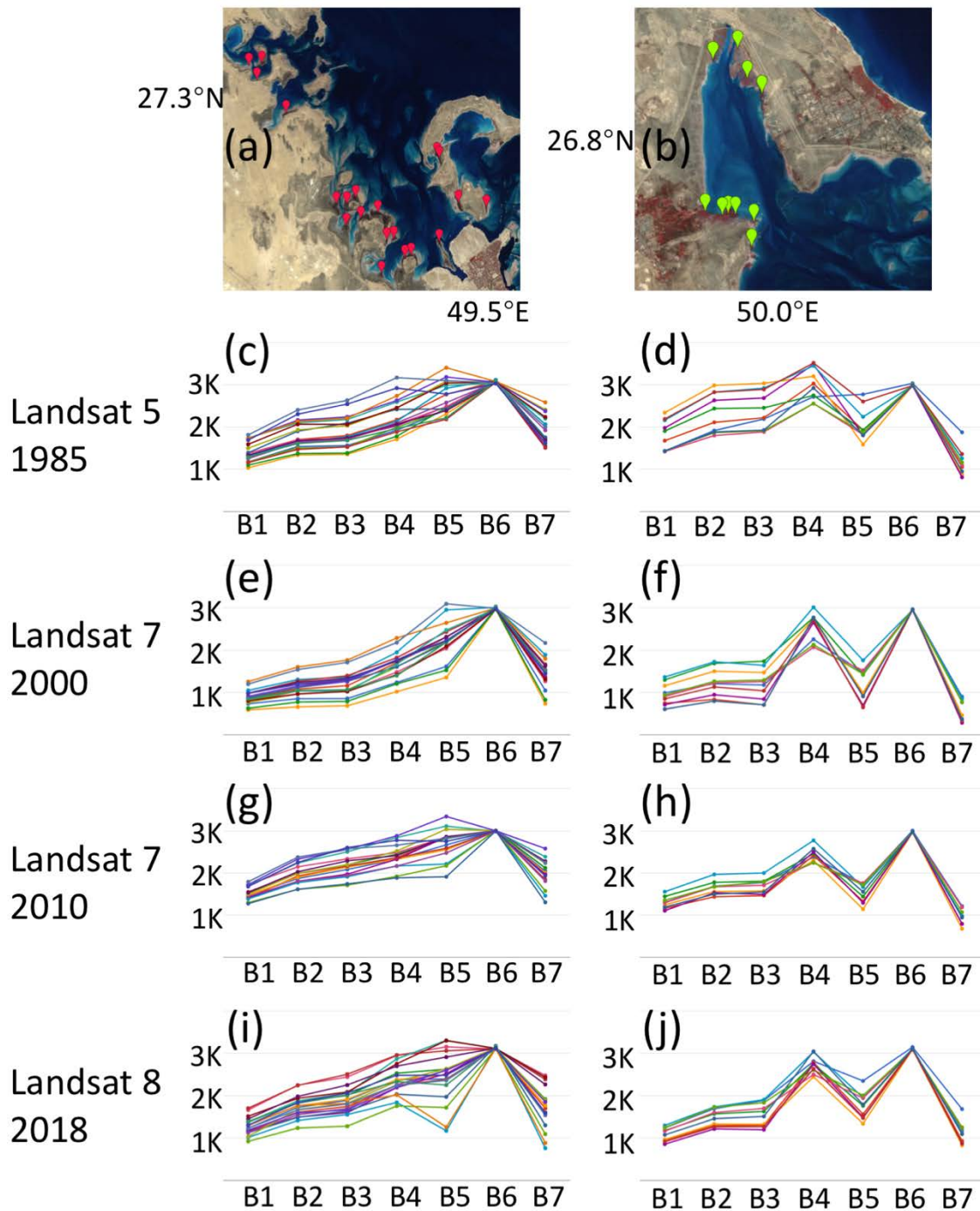
359

360 **3. Results and discussion**

361 *3.1 Comparison of existing mangrove datasets*

362 Spectral analysis was conducted here to evaluate the data accuracy across different
363 sources. Mangroves spectral signature is quite unique and has been correctly identified,
364 used and compared with other sources to avoid misclassification with other marine
365 habitats, namely salt marshes and macro algae (Benson et al., 2017; Corcoran et al., 2007;
366 Giri, 2016; Ranjan et al., 2017). The left panel of Fig.2 shows the spectral signature of
367 end members from the mangrove habitat only identified by USGS Global Mangrove
368 Forest Distribution dataset (red points in Fig. 2a). They are displayed as Landsat 5 image
369 of 1985 in Fig. 2c, the Landsat 7 images of 2000 in Fig. 2e and 2010 in Fig. 2g, and

370 Landsat 8 image of 2018 in Fig. 2i. The right panel of Fig. 2 shows the spectral signature
371 of samples from mangrove habitat agreed by all of three datasets (green points in Fig. 2b).
372 They are displayed as the Landsat 5 image of 1985 in Fig. 2d, the Landsat 7 images of
373 2000 in Fig. 2f and 2010 in Fig. 2h, and Landsat 8 image of 2018 in Fig. 2j. It is
374 noteworthy that the bands in Landsat 8 are renamed to have the same spectral range of
375 Landsat 5 and Landsat 7. It is quite evident that the spectral distributions are coherent as
376 shown in Figs. 2(d, f, h and j), with high value at band 4 and lower value at band 5 and
377 band 7. However, Figs. 2(c, e, g and i) does not show the same pattern – band 5 value is
378 always higher than the value of band 4 which should not be the case. From the above and
379 based on the conducted spectral analysis using a wide range of endmembers and
380 comparing with established research, we believe that USGS data overestimated mangrove
381 habitats distribution. On the other hand, the data obtained from Saudi Aramco (Loughland
382 and Al-Abdulkader, 2011) shows the misclassified locations in the USGS dataset as
383 saltmarsh habitats. The Landsat 5 data in 1985 was able to distinguish saltmarsh from
384 mangroves, which is even more accurate for Landsat 7 & 8. This is because in Landsat 7
385 & 8 the values of each band show more distinctive behavior as compared to Landsat 5
386 images, where all bands show less distinction Figs. 2(d, f, h and j). Considering these
387 differences and facts between these sensors, we opted to perform the change detection
388 analysis on the mangroves habitats using Landsat 7&8 data.



389
 390 Figure 2. Endmembers selection for spectral reflectance analysis using red and green points over (a) Jubail
 391 Conservation; (b) Tarut Bay. Red locations: classified as Mangrove forests according to USGS dataset only
 392 and Green locations: classified as Mangrove forests according to all three datasets with spectral profiles (c
 393 & d), (e & f), (g & h), (i & j) for 1985 Landsat 5, 2000 Landsat 7, 2010 Landsat 7, and 2018 Landsat 8
 394 images, respectively.

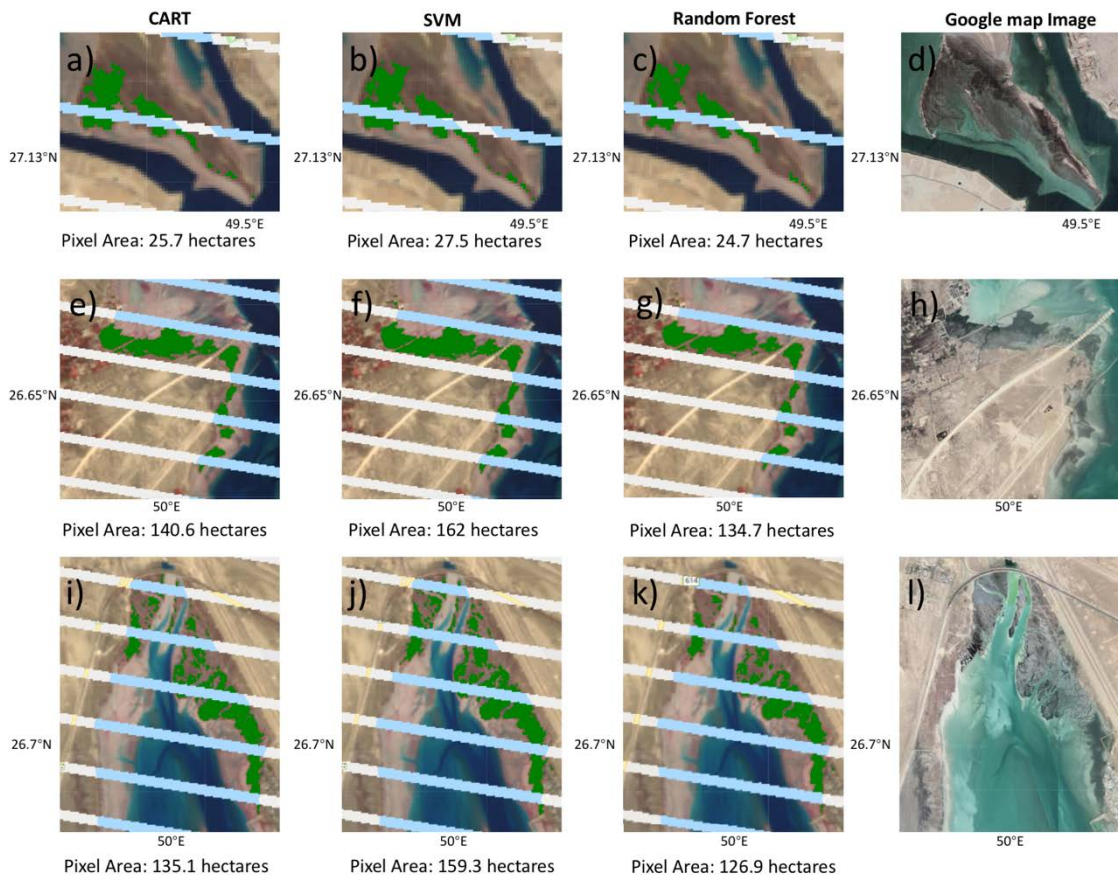
395

396 *3.2 Mangrove change detection*

397 The supervised classification models used in this study (i.e. CART, SVM and RF)
398 were built using the same training datasets from Landsat 7 (all samples from non-gap
399 areas) and Landsat 8 images during 2018. Five different categories, namely: arid land,
400 mangrove, tidal flat, saltmarshes and water body were identified using 30 sample
401 observation points per category to ensure accuracy. Training datasets accuracy was
402 assessed against new testing datasets through computing the confusion matrix for each
403 model. In this work we looked at the “trainAccuracy” parameter that describes how well
404 the classifier was able to correctly label resubstituted training data (i.e. data
405 the classifier had already seen). However, to get a true validation accuracy, we showed
406 our three classifiers a new ‘testing’ data and applied the classifiers to the new testing data
407 to assess the “errorMatrix” for this withheld validation data. The accuracy values ranged
408 from > 95% for CART and > 90% for others, being applied on both Landsat 7 & 8.

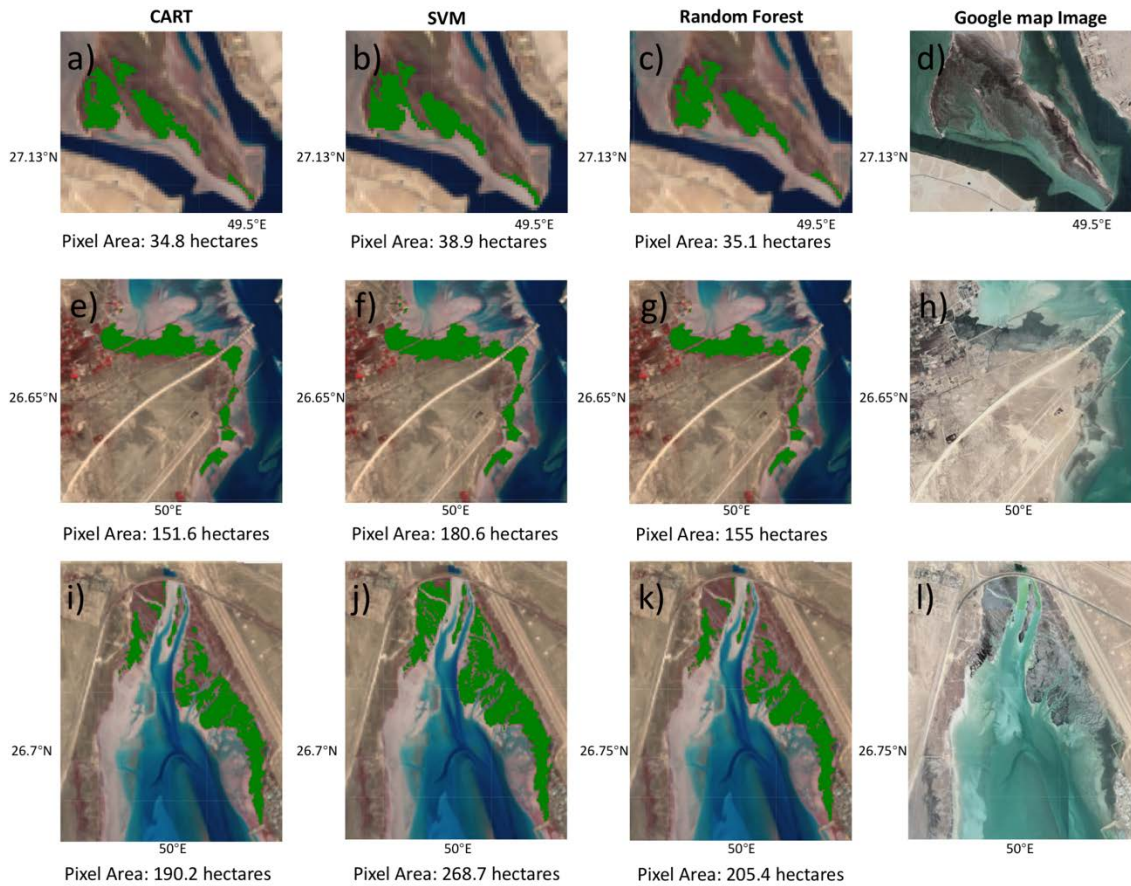
409 The mangrove forests distribution following the three models are shown using
410 Landsat 7 & 8 in the Gurmah Island (GI) (Figs. 3 & 4(a, b and c), North Middle Tarut
411 Bay (NMTB) (Figs. 3 & 4(e, f and g)), and North Tarut Bay (NTB) (Figs. 3 & 4(i, j and
412 k) during 2018, respectively. High resolution true color images from Google Map were
413 included for comparison (Figs. 3 & 4 (d, h and l). The resulting pixel coverage for
414 mangrove forests based on three classifiers, after vegetation mask ($NDVI > 0.15$) was
415 applied, is computed and presented for each location. The areas of the classified
416 mangroves (in hectares) for Landsat 7 were: SVM (GI: 27.5, NMTB: 162, NTB: 159.3) >
417 CART (GI: 25.7, NMTB: 140.6, NTB: 135.1) > Random Forest (GI: 24.6, NMTB: 97,
418 NTB: 111.5) and for Landsat 8 were: SVM (GI: 38.9, NMTB: 180.6, NTB: 268.7) >
419 CART (GI: 34.8, NMTB: 151.6, NTB: 190.2) > Random Forest (GI: 31.6, NMTB: 150.5,
420 NTB: 183.8). It is clear that SVM classifier overestimated the distribution while RF
421 underestimated it. The three models successfully showed similar mangrove distribution

422 over the different locations and using Landsat 7 & 8 datasets, yet we believe that CART
 423 showed the most accurate pixel coverage counting and best performance. Higher pixel
 424 coverage is expected from Landsat 8 images (Fig. 4) due to the absence of gaps exhibited
 425 in Landsat 7 data (Fig. 3). The variance in the pixel coverage following the three
 426 classifiers can be attributed to the sparse growth of mangrove habitats along coastlines,
 427 as seen from the high resolution true color composites, yet SVM failed to identify this
 428 sparsity and hence overestimated and RF did the opposite. Given the CART model higher
 429 performance and accuracy, it is now selected for the mangrove change detection analysis.



430
431

432 Figure 3. Supervised classification results of Landsat 7 image of 2018 for the mangrove forests (green area)
 433 and corresponding mangrove coverage (in hectares) using CART (a, e, i), SVM (b, f, j), RF (c, g, k),
 434 compared with high resolution true colour Google Map image (d, h, l), for GI(a-d), NMTB(e-h) and NTB(i-
 435 l)



436

437 Figure 4. Supervised classification results of Landsat 8 image of 2018 for the mangrove forests (green area)
 438 and corresponding mangrove coverage (in hectares) using CART (a, e, i), SVM (b, f, j), RF (c, g, k),
 439 compared with high resolution true colour Google Map image (d, h, l), for GI(a-d), NMTB(e-h) and NTB(i-
 440 l)

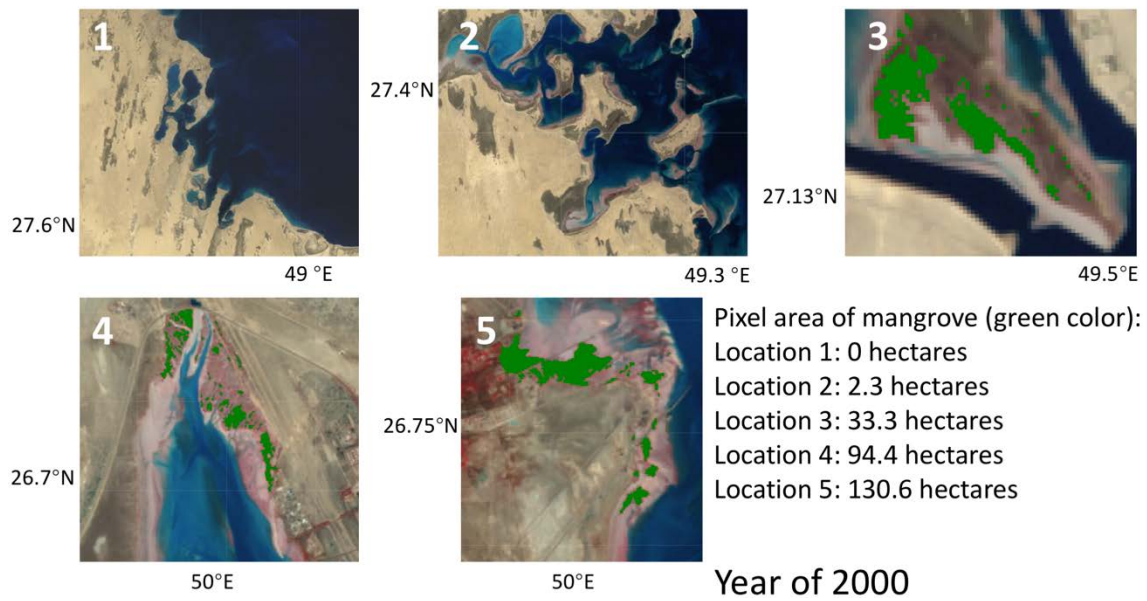
441 Change detection analysis is performed between 2000 and 2010 using the CART
 442 classifier based images for Landsat 7, after sub-setting our data to the previously
 443 mentioned five locations (Fig. 1) and masking terrestrial vegetation, land and water for
 444 classification purposes. Masking of terrestrial vegetation was crucial for the classification
 445 accuracy and to avoid overestimation errors by the classifiers. Landsat 7 is specifically
 446 selected against Landsat 8 to look at the change starting 2000 rather than 2013. Figs. 5 &
 447 6 shows that regions 1 (Manifah) and 2 (Al-Khair) already with small mangroves fraction
 448 (0 and 2.3 hectares) in 2000 exhibits almost little to no change in 2010. It is noteworthy
 449 that an artificial island was built in region 1, for ship docking and tourists (Fig. 6, region

450 1). Alternatively, regions 3 (GI) and 5 (NMTB), with the larger mangrove distribution
451 (33.3 and 130.6 hectares) in 2000, showed an expected decline during 2010. This may be
452 due to coastal developments and surrounding human activities (Amin et al., 2018).

453 The observed increase of 0.21 km² over the mangrove habits in the northern Tarut
454 Bay and Tarut Island from 2.25 km² to 2.46 km² during the period 2000-2010 matched
455 the reported areal increase of 1.4 km² observed from 1999 (4 km²) (Khan and Kumar
456 2009) to 2011 (5.4 km²) (Almahasheer et al., 2013) for the whole Tarut Bay. Moreover,
457 the increase of 1.14 km² between 2010 (2.46 km²) and 2018 (3.6 km²) also agrees with
458 the increasing trend of the Tarut Bay mangrove habitats from 2011 to 2014 (Al-Ali et al.
459 2015). However, we believe that data SLC gaps, shown as empty clear stripes, also played
460 a role in this observation. As for region 4 (NTB) the mangrove coverage increased from
461 (94.4 hectares) in 2000 to (117.9 hectares) in 2010. It is highly likely that these
462 classification results using gap-filled image by GEE mosaicking method contributed to
463 this increase in the mangroves distribution that was validated with ground observations
464 over some of the gap areas (Fig.6, region 4). It is clear that mangrove biomass and
465 distribution in NTB has unexpectedly increased from 94.4 to 117.9 to 190.2 hectares
466 during 2000 (Fig.5 region 4), 2010 (Fig. 6 region 4) and 2018 (Fig. 4i). Data filling may
467 have contributed to better accuracy; however, tide levels also affect mangroves that is
468 evident from their divergent spectral properties in high/low water levels. This will be
469 discussed further in the next section.

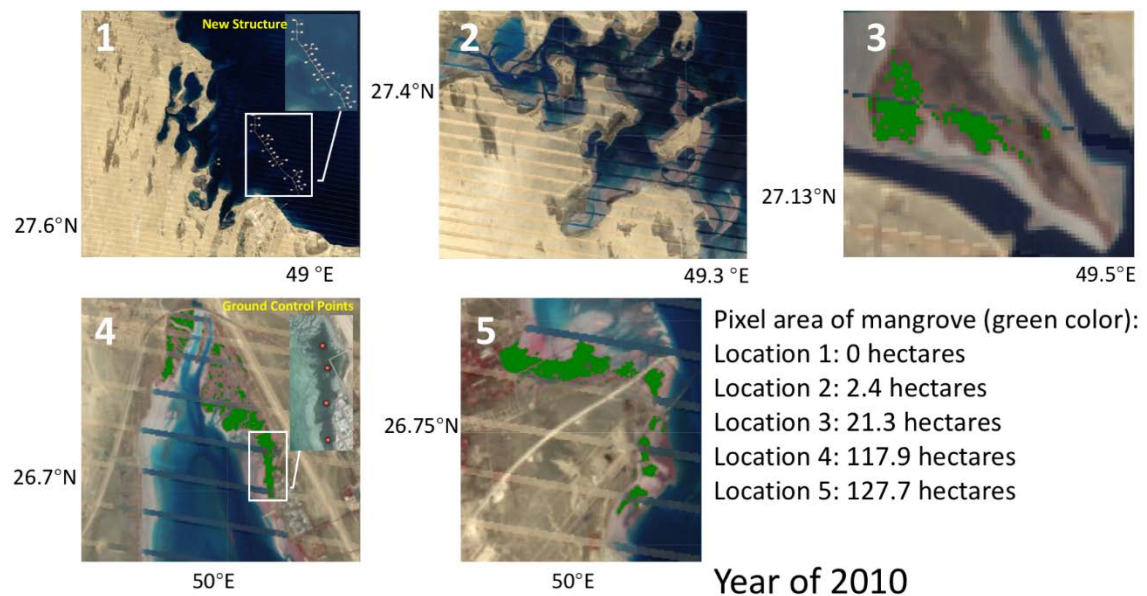
470

471



472

473 Figure 5. Mangrove forest distribution (green area) using the CART classifier applied on Landsat 7 year
 474 2000. The text at the right panel lists the mangrove area for each location (1-5). Refer to Fig.1 for
 475 regions.



476

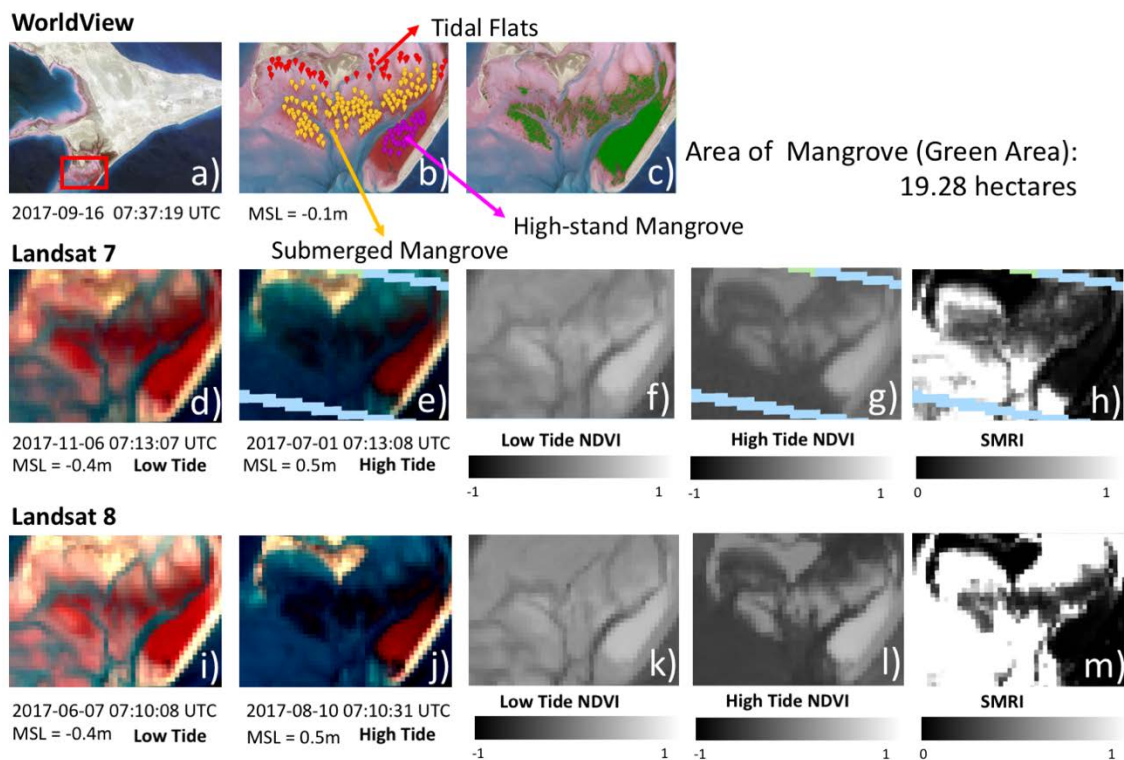
477 Figure 6. Mangrove forest distribution (green area) using the CART classifier applied on Landsat 7 year
 478 2010. The text at the right panel lists the mangrove area for each location (1-5). Refer to Fig.1 for regions.
 479

480 3.3 Submerged mangrove detection

481 As mentioned above, tidal levels could have an impact on mangrove mapping and
 482 detection. SMRI was generated from low and high tides on the Abu Ali Island located in

483 region 3 (Jubail), to use the unique spectral signature of submerged mangroves forest to
484 distinguish them by different tide levels. The WorldView-2 high resolution images of
485 Abu Ali Island show mangrove forests in the south coast highlighted by the red square
486 (Fig. 7a). Fig. 7b shows the sample points for dense high-stand mangroves in the south
487 east corner (magenta points), tidal submerged mangrove in the middle (orange points),
488 and tidal flats (red points). The mangroves total area, including tidal and non-tidal areas,
489 was calculated using the K-means classification method applied on Fig. 7b and was found
490 to be 19.28 hectares (see green area in Fig. 7c). To assess tidal impacts on mangrove
491 distribution, the mean sea level (MSL) data was also used, mentioned above in the data
492 section. False color composites for the region at low tides (MSL = -0.4m) and high tides
493 (MSL = 0.5) are shown in Figs. 7(d & e) for Landsat 7 and Figs. 7(i & j) for Landsat 8,
494 respectively. It is noteworthy that Landsat 7 SLC failure gaps did not intercede the areas
495 of mangrove forests in the case of Abu Ali Island. Figs. 7(d & i) representing mangroves
496 at low tides (marked as the red vegetation) from Landsat 7 & 8 exhibits larger distribution
497 than the submerged mangroves that almost disappeared during the high tides (Figs. 7(e &
498 j). This indicates that change detection analysis of such area could be dramatically altered
499 if images are not compared at the same water level. The NDVI images of low tides (Figs.
500 7f & 7k), and high tides (Figs. 7g & 7l) show that the NDVI index could be helpful to
501 distinguish high-stand mangrove from others, but fails to discriminate the submerged
502 mangroves and tidal flats in low tides, as well as submerged mangrove and land. While
503 in the SMRI images (Figs. 7h & 7m), submerged mangroves could be seen as grey areas.
504 The SMRI images indicate that: 1) for non-tidal regions such as land or high-stand
505 mangrove, the SMRI value is close to 0; 2) for non-vegetation tidal flats regions, the
506 SMRI value could be very high above 1 (Fig. 7m), but also could be closer to submerged

507 mangrove. One can use the spectral properties of submerged mangrove and tidal flats
 508 under high tides condition to separate them.

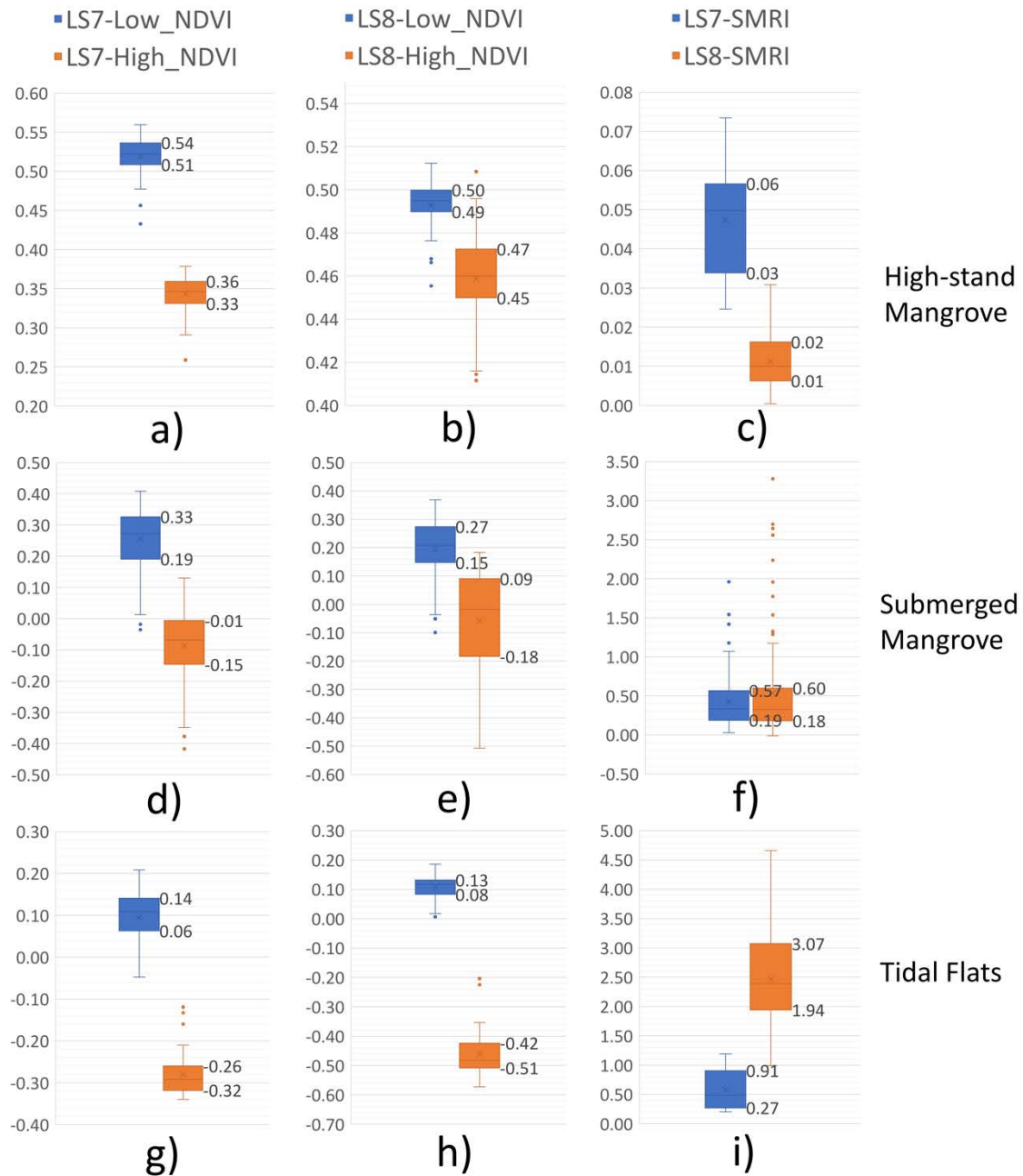


509 Figure 7. WorldView-2 image of Abu Ali Island: (a) the mangrove forest in red square; (b) Sample points
 510 for tidal flats (red), high-stand mangroves (orange) and submerged mangrove (magenta); (c) Total
 511 mangrove area (green area). Landsat 7 and 8 images: (d, i) low tide; (e, j) high tide; (f, k) NDVI of low tide;
 512 (g, l) NDVI of high tide; (h, m) SMRI, respectively.

513

514 Figure 8 exhibits the ranges of NDVI and SMRI values of the samples for high-stand
 515 mangrove (Figs. 8a-c), submerged mangrove (Figs. 8d-e) and tidal flats (Figs. 8g-i) in
 516 Landsat 7&8 images displayed in Fig. 7. The NDVI values in low tides are higher than
 517 those in high tides in general. However, NDVI values of Landsat 8 images between tide
 518 levels are very close as seen in Fig. 8b. In the Fig. 8f, the SMRI values have very similar
 519 ranges (0.18 to 0.60 and 0.19 to 0.57) regardless of the different satellite images. This
 520 proves the robustness of SMRI as a submerged mangrove detection method. However,
 521 the ranges of SMRI values for Landsat 7 are overlapped between submerged mangroves

522 and tidal flats (Fig. 8f and 8i). This could be solved by applying the divergence of high
 523 tide NDVI values for submerged mangrove (-0.18 to 0.09 in Fig. 8e) and tidal flats (-0.51
 524 to -0.42) in Fig. 8h), which could be used to mask out tidal flats from SMRI-indicated
 525 mangrove areas.

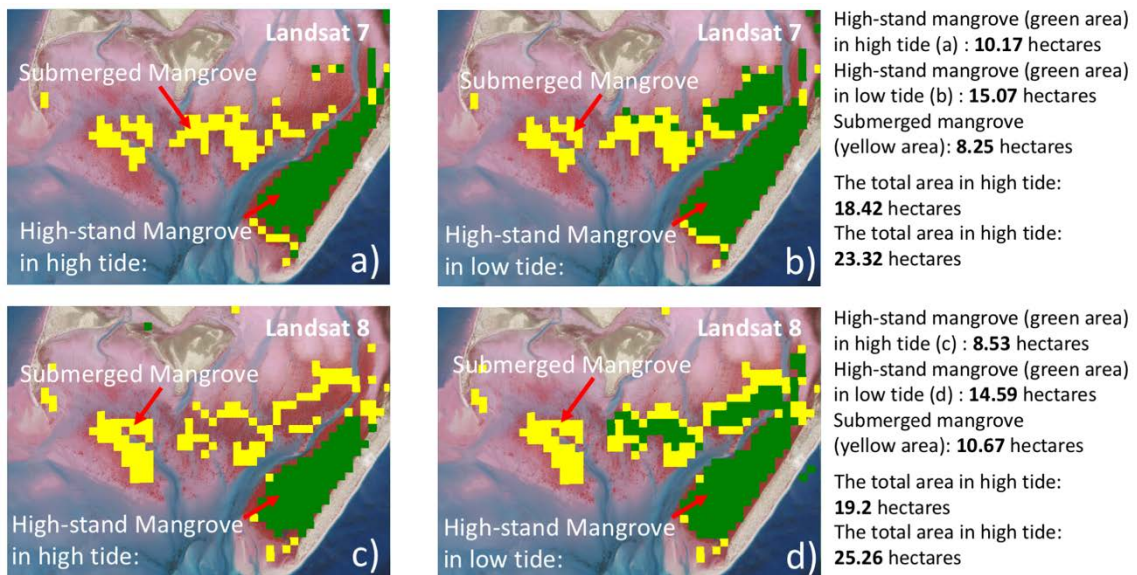


526
 527 Figure 8. First two columns: Range of NDVI values of the samples for high-stand mangrove (a,b),
 528 submerged mangrove (d,e) and tidal flats (g,h) for low tides (blue) and high tides (orange) of Landsat 7 and

529 8 images in Fig. 7. Third column: Range of SMRI values of the samples for high-stand mangrove (c),
 530 submerged mangrove (f) and tidal flats (i) for Landsat 7 (blue) and Landsat 8 (orange) images in Fig. 7.

531 Figure 9 shows the detection results for both high-stand mangrove as green areas
 532 using K-means unsupervised method, and submerged mangrove as yellow areas by
 533 choosing regions with SMRI values (0.18 to 0.60 for Landsat 7, 0.19 to 0.57 for Landsat
 534 8, then masking with high tide NDVI > -0.2). The areas of submerged mangroves are 8.25
 535 and 10.67 hectares for Landsat 7 and Landsat 8 images, respectively. The classified
 536 mangrove areas of Figs. 9(b & d) cover most of the targeted mangrove areas shown in the
 537 background using the high resolution WorldView-2 image. The summation of high-stand
 538 mangrove in high tide and submerged mangrove areas (19.2 hectares using Landsat 8,
 539 18.42 hectares using Landsat 7) are very close to high resolution WorldView-2 image
 540 result (19.28 hectares), indicating that this approach could provide an effective estimate
 541 and addresses the tidal impact on mangrove mapping.

542



543 Figure 9. (a) High-stand mangrove forests (green area) in high tide of Fig. 7e; SMRI indicated submerged
 544 mangrove forests (yellow area). (b) High-stand mangrove forests (green area) in low tide of Fig. 7d; same
 545 submerged mangrove forests as Fig. 9a. (d) High-stand mangrove forests (green area) and in high tide of
 546 Fig. 7j; SMRI indicated submerged mangrove forests (yellow area). (b) High-stand mangrove forests (green
 547

548 area) in low tide of Fig. 7i; same submerged mangrove forests as Fig. 9c. The text at the very right panel
549 lists the mangrove area.

550

551 **4. Conclusions**

552 The spatial distribution and spatial-temporal changes of mangrove forests in Arabian
553 Gulf along the Saudi Arabia during the period of 2000 to 2018 were explored using large
554 data sets and spatial analysis. First, we compared the spectral reflectance signatures
555 between identified mangrove forest and other coastal vegetation habitats (such as
556 seagrasses and saltmarshes) using Landsat 5&7&8 data. Mangrove habitat detection in
557 the WAG was carried out through the evaluation of the three widely-used mangrove
558 classification methods, namely Supported Vector Machine (SVM), Classification and
559 Regression Trees (CART) and Random Forest (RF). CART was validated as the most
560 effective classifier (accuracy > 95%) for WAG mangrove detestation. Later, we used the
561 medium-resolution Landsat 7&8 images to build a CART-based mangrove supervised
562 classification model to obtain mangrove areas and distributions for 2000, 2010 and 2018.
563 With both Landsat and the high resolution WorldView-2 images, the new SMRI method
564 was applied in the area of Abu Ali Islands with the usage of K-means unsupervised
565 method to identify and evaluate the biomass and distribution of submerged mangroves in
566 the tidal area. We investigated the protocol to detect overall mangrove distribution from
567 samples taken from Abu Ali Island with indices SMRI and NDVI values generated from
568 Landsat 7&8 images. By employing these two indices, there was a good match between
569 the estimates of the mangrove area to the south of Abu Ali Island at 19.20 hectares using
570 Landsat 8 and 19.28 hectares calculated from the high resolution WorldView-2. This
571 studies presents a unique approach of SMRI to detect mangroves with historical Landsat
572 images that has historical record and can be used to address tidal impacts on mangrove

573 mapping and areas estimation over different locations, which could achieve more accurate
574 outcomes of mangrove detection within limited usage of costly high resolution remote
575 sensing imagery.

576

577 **Acknowledgements**

578 The authors would like to acknowledge the use of the Samueli Laboratory in
579 Computational Sciences in the Schmid College of Science and Technology, Chapman
580 University for data processing and analysis. We would also like to acknowledge the
581 Center for Environment and Water, King Fahd University of Petroleum and Minerals
582 (KFUPM), Saudi Arabia for conducting field measurements for use in further
583 comparisons and validations studies. Jingjing Li would also like to acknowledge the
584 support through the NASA Minority University Research and Education Project
585 (MUREP) Institutional Research Opportunity grant number [NNX15AQ06A].

586

587 **References**

588 Ahamed, T., Tian, L., Zhang, Y., Ting, K.C., 2011. A review of remote sensing methods
589 for biomass feedstock production. *Biomass and Bioenergy* 35, 2455–2469.
590 <https://doi.org/10.1016/j.biombioe.2011.02.028>

591 Al-Ali, A. M., Del Campo, A. G., & Rocha, C., 2015. Environmental assessment of
592 mangrove communities in Tarut bay, eastern Arabian Peninsula, based on
593 multidisciplinary approach. In *International Archives of the Photogrammetry, Remote*
594 *Sensing and Spatial Information Sciences—ISPRS Archives*, (7W3 ed., Vol. 40, pp. 269–
595 276). <https://doi.org/10.5194/isprsarchives-XL-7-W3-269-2015>.

596 Al-Kahtany, K., El-Sorogy, A., Al-Kahtany, F., Youssef, M., 2018. Heavy metals in
597 mangrove sediments of the central Arabian Gulf shoreline, Saudi Arabia. *Arabian Journal*
598 *of Geosciences* 11. <https://doi.org/10.1007/s12517-018-3463-0>

599 Almahasheer, H., 2019. High levels of heavy metals in Western Arabian Gulf mangrove
600 soils. *Molecular Biology Reports*. <https://doi.org/10.1007/s11033-019-04603-2>

601 Almahasheer, H., 2018. Spatial coverage of mangrove communities in the Arabian Gulf.
602 *Environmental Monitoring and Assessment* 190. [https://doi.org/10.1007/s10661-018-](https://doi.org/10.1007/s10661-018-6472-2)
603 [6472-2](https://doi.org/10.1007/s10661-018-6472-2).

604 Almahasheer, H., Aljowair, A., Duarte, C.M., Irigoien, X., 2016. Decadal stability of Red
605 Sea mangroves. *Estuarine, Coastal and Shelf Science* 169, 164–172.
606 <https://doi.org/10.1016/j.ecss.2015.11.027>

607 Almahasheer, H., Al-Taisan, W., Mohamed, M. K., 2013. Mangrove deterioration in
608 Tarut Bay on the Eastern Province of the Kingdom of Saudi Arabia. *Pakhtunkhwa Journal*
609 *Life Sciences* 01, 49–59.

610 Al-Maslamani, I., Walton, M.E.M., Kennedy, H.A., Al-Mohannadi, M., Le Vay, L.,
611 2013. Are mangroves in arid environments isolated systems? Life-history and evidence
612 of dietary contribution from inwelling in a mangrove-resident shrimp species. *Estuarine,*
613 *Coastal and Shelf Science* 124, 56–63. <https://doi.org/10.1016/j.ecss.2013.03.007>

614 Al-Muzaini, S., Jacob, P.G., 1996. Marine plants of the Arabian Gulf. *Environment*
615 *International* 22, 369–376. [https://doi.org/10.1016/0160-4120\(96\)00023-2](https://doi.org/10.1016/0160-4120(96)00023-2)

616 Alongi, D.M., 2002. Present state and future of the world's mangrove forests.
617 *Environmental Conservation* 29. <https://doi.org/10.1017/S0376892902000231>

618 Althukair, A., Khan, M., & Alhinai, K., 1995. Monitoring of coast line and habitat
619 changes of Tarut Bay, Saudi Arabia using satellite images. *Proceedings of ASCE-SAS*
620 *Second Regional Conference and Exhibition*.

621 Amin, S., Fouad, M., Ataisan, W., Zyadah, M., n.d. Human, Urban and Environmental-
622 Induced Alterations in Mangroves Pattern along Arabian Gulf Coast, Eastern Province,
623 KSA. <https://doi.org/10.20944/preprints201801.0259.v1>

624 Assessment, M.E. Millennium Ecosystem Assessment Findings; Millennium Ecosystem
625 Assessment: Washington, DC, USA, 2005. 9

626 Benson, L., Glass, L., Jones, T., Ravaoarinosihoarana, L., Rakotomahazo, C., 2017.
627 Mangrove Carbon Stocks and Ecosystem Cover Dynamics in Southwest Madagascar and
628 the Implications for Local Management. *Forests* 8, 190. <https://doi.org/10.3390/f8060190>

629 Bird, E., 2010. Saudi Arabia, Persian Gulf Coast, in: Bird, E.C.F. (Ed.), Encyclopedia of
630 the World's Coastal Landforms. Springer Netherlands, Dordrecht, pp. 1045–1046.
631 https://doi.org/10.1007/978-1-4020-8639-7_194

632 Breiman, L. (Ed.), 1998. Classification and regression trees, Repr. ed. Chapman & Hall
633 [u.a.], Boca Raton.

634 Burt, J.A., 2014. The environmental costs of coastal urbanization in the Arabian Gulf.
635 City 18, 760–770. <https://doi.org/10.1080/13604813.2014.962889>

636 Collins, D.S., Avdis, A., Allison, P.A., Johnson, H.D., Hill, J., Piggott, M.D., Hassan,
637 M.H.A., Damit, A.R., 2017. Tidal dynamics and mangrove carbon sequestration during
638 the Oligo–Miocene in the South China Sea. Nature Communications 8, 15698.
639 <https://doi.org/10.1038/ncomms15698>

640 Corcoran, E., Ravilious, C., Skuja, M., 2007. Mangroves of Western and Central Africa.
641 UNEP-WCMC Biodiversity Series (UNEP)

642 Danielsen, F., 2005. The Asian Tsunami: A Protective Role for Coastal Vegetation.
643 Science 310, 643–643. <https://doi.org/10.1126/science.1118387>

644 Dinesh, R., Ghoshal Chaudhuri, S., 2013. Soil biochemical/microbial indices as
645 ecological indicators of land use change in mangrove forests. Ecological Indicators 32,
646 253–258. <https://doi.org/10.1016/j.ecolind.2013.03.035>

647 Donato, D.C., Kauffman, J.B., Murdiyarto, D., Kurnianto, S., Stidham, M., Kanninen,
648 M., 2011. Mangroves among the most carbon-rich forests in the tropics. Nature
649 Geoscience 4, 293–297. <https://doi.org/10.1038/ngeo1123>

650 Duke, N.C., Meynecke, J.-O., Dittmann, S., Ellison, A.M., Anger, K., Berger, U.,
651 Cannicci, S., Diele, K., Ewel, K.C., Field, C.D., Koedam, N., Lee, S.Y., Marchand, C.,
652 Nordhaus, I., Dahdouh-Guebas, F., 2007. A World Without Mangroves? Science 317,
653 41b-42b. <https://doi.org/10.1126/science.317.5834.41b>

654 Duro, D.C., Franklin, S.E., Dubé, M.G., 2012. A comparison of pixel-based and object-
655 based image analysis with selected machine learning algorithms for the classification of
656 agricultural landscapes using SPOT-5 HRG imagery. Remote Sensing of Environment
657 118, 259–272. <https://doi.org/10.1016/j.rse.2011.11.020>

658 El-Askary, H., El-Mawla, S.H.A., Li, J., El-Hattab, M.M., El-Raey, M., 2014. Change
659 detection of coral reef habitat using Landsat-5 TM, Landsat 7 ETM+ and Landsat 8 OLI
660 data in the Red Sea (Hurghada, Egypt). *International Journal of Remote Sensing* 35,
661 2327–2346. <https://doi.org/10.1080/01431161.2014.894656>Ellis, W.L., Bell, S.S., 2013.
662 Intertidal fish communities may make poor indicators of environmental quality: Lessons
663 from a study of mangrove habitat modification. *Ecological Indicators* 24, 421–430.
664 <https://doi.org/10.1016/j.ecolind.2012.07.008>

665 Faridah-Hanum, I., Yusoff, F.M., Fitrianto, A., Ainuddin, N.A., Gandaseca, S., Zaiton,
666 S., Norizah, K., Nurhidayu, S., Roslan, M.K., Hakeem, K.R., Shamsuddin, I., Adnan, I.,
667 Awang Noor, A.G., Balqis, A.R.S., Rhyma, P.P., Siti Aminah, I., Hilaluddin, F., Fatin,
668 R., Harun, N.Z.N., 2019. Development of a comprehensive mangrove quality index
669 (MQI) in Matang Mangrove: Assessing mangrove ecosystem health. *Ecological*
670 *Indicators* 102, 103–117. <https://doi.org/10.1016/j.ecolind.2019.02.030>

671 Foody, G.M., Mathur, A., 2006. The use of small training sets containing mixed pixels
672 for accurate hard image classification: Training on mixed spectral responses for
673 classification by a SVM. *Remote Sensing of Environment* 103, 179–189.
674 <https://doi.org/10.1016/j.rse.2006.04.001>

675 Green, E.P., Mumby, P.J., Edwards, A.J., Clark, C.D. and Ellis, A.C., 1998. The
676 assessment of mangrove areas using high resolution multispectral airborne
677 imagery. *Journal of Coastal Research*, 433-443.

678 Giri, C., 2016. Observation and Monitoring of Mangrove Forests Using Remote Sensing:
679 Opportunities and Challenges. *Remote Sensing* 8, 783. <https://doi.org/10.3390/rs8090783>

680 Giri, C., Long, J., Abbas, S., Murali, R.M., Qamer, F.M., Pengra, B., Thau, D., 2015.
681 Distribution and dynamics of mangrove forests of South Asia. *Journal of Environmental*
682 *Management* 148, 101–111. <https://doi.org/10.1016/j.jenvman.2014.01.020>

683 Giri, C., Ochieng, E., Tieszen, L.L., Zhu, Z., Singh, A., Loveland, T., Masek, J., Duke,
684 N., 2011. Status and distribution of mangrove forests of the world using earth observation
685 satellite data: Status and distributions of global mangroves. *Global Ecology and*
686 *Biogeography* 20, 154–159. <https://doi.org/10.1111/j.1466-8238.2010.00584.x>

687 Gitelson, A.A., Kaufman, Y.J., Merzlyak, M.N., 1996. Use of a green channel in remote
688 sensing of global vegetation from EOS-MODIS. *Remote Sensing of Environment* 58,
689 289–298. [https://doi.org/10.1016/S0034-4257\(96\)00072-7](https://doi.org/10.1016/S0034-4257(96)00072-7)

690 Heenkenda, M., Joyce, K., Maier, S., Bartolo, R., 2014. Mangrove Species Identification:
691 Comparing WorldView-2 with Aerial Photographs. *Remote Sensing* 6, 6064–6088.
692 <https://doi.org/10.3390/rs6076064>

693 Heenkenda, M.K., Joyce, K.E., Maier, S.W., de Bruin, S., 2015. Quantifying mangrove
694 chlorophyll from high spatial resolution imagery. *ISPRS Journal of Photogrammetry and*
695 *Remote Sensing* 108, 234–244. <https://doi.org/10.1016/j.isprsjprs.2015.08.003>

696 Heumann, B.W., 2011. An Object-Based Classification of Mangroves Using a Hybrid
697 Decision Tree—Support Vector Machine Approach. *Remote Sensing* 3, 2440–2460.
698 <https://doi.org/10.3390/rs3112440>

699 Hutchison, J., Manica, A., Swetnam, R., Balmford, A., Spalding, M., 2014. Predicting
700 Global Patterns in Mangrove Forest Biomass: Global patterns in mangrove biomass.
701 *Conservation Letters* 7, 233–240. <https://doi.org/10.1111/conl.12060>

702 Kanniah, K., Sheikhi, A., Cracknell, A., Goh, H., Tan, K., Ho, C., Rasli, F., 2015. Satellite
703 Images for Monitoring Mangrove Cover Changes in a Fast Growing Economic Region in
704 Southern Peninsular Malaysia. *Remote Sensing* 7, 14360–14385.
705 <https://doi.org/10.3390/rs71114360>

706 Kathiresan, K., Rajendran, N., 2005. Coastal mangrove forests mitigated tsunami.
707 *Estuarine, Coastal and Shelf Science* 65, 601–606.
708 <https://doi.org/10.1016/j.ecss.2005.06.022>

709 Khan, M. A., Kumar, A., 2009. Impact of “urban development” on mangrove forests
710 along the west coast of the Arabian Gulf. *E-journal Earth Science India* 2, 159–173

711 Kim, S.-R., Prasad, A.K., El-Askary, H., Lee, W.-K., Kwak, D.-A., Lee, S.-H., Kafatos,
712 M., 2014. Application of the Savitzky-Golay Filter to Land Cover Classification Using
713 Temporal MODIS Vegetation Indices. *Photogrammetric Engineering & Remote Sensing*
714 80, 675–685. <https://doi.org/10.14358/PERS.80.7.675>

715 Lawrence, R.L., and Andrea, W., 2001. "Rule-based classification systems using
716 classification and regression tree (CART) analysis." *Photogrammetric engineering and*
717 *remote sensing* 67.10: 1137-1142.

718 Le Louarn, M., Clergeau, P., Briche, E., Deschamps-Cottin, M., 2017. "Kill Two Birds
719 with One Stone": Urban Tree Species Classification Using Bi-Temporal Pléiades Images
720 to Study Nesting Preferences of an Invasive Bird. *Remote Sensing* 9, 916.
721 <https://doi.org/10.3390/rs9090916>

722 Li, M.S., Mao, L.J., Shen, W.J., Liu, S.Q., Wei, A.S., 2013. Change and fragmentation
723 trends of Zhanjiang mangrove forests in southern China using multi-temporal Landsat
724 imagery (1977–2010). *Estuarine, Coastal and Shelf Science* 130, 111–120.
725 <https://doi.org/10.1016/j.ecss.2013.03.023>

726 Li, M., Ma, L., Blaschke, T., Cheng, L., Tiede, D., 2016. A systematic comparison of
727 different object-based classification techniques using high spatial resolution imagery in
728 agricultural environments. *International Journal of Applied Earth Observation and*
729 *Geoinformation* 49, 87–98. <https://doi.org/10.1016/j.jag.2016.01.011>

730 Li, W., El-Askary, H., ManiKandan, K., Qurban, M., Garay, M., Kalashnikova, O., 2017.
731 Synergistic Use of Remote Sensing and Modeling to Assess an Anomalously High
732 Chlorophyll-a Event during Summer 2015 in the South Central Red Sea. *Remote Sensing*
733 9, 778. <https://doi.org/10.3390/rs9080778>

734 Li, W., El-Askary, H., Qurban, M., Proestakis, E., Garay, M., Kalashnikova, O., Amiridis,
735 V., Gkikas, A., Marinou, E., Piechota, T., Manikandan, K., 2018. An Assessment of
736 Atmospheric and Meteorological Factors Regulating Red Sea Phytoplankton Growth.
737 *Remote Sensing* 10, 673. <https://doi.org/10.3390/rs10050673>

738 Loughland, R.A., Al-Abdulkader, K.A., 2011. *Marine atlas, Western Arabian Gulf*. Saudi
739 Aramco, Environment Protection Dept. : Center for Environment & Water Research
740 Institute, KFUPM, Dhahran, Saudi Arabia

741 Moore, G.E., Grizzle, R.E., Ward, K.M., Alshihi, R.M., 2015. Distribution, Pore-Water
742 Chemistry, and Stand Characteristics of the Mangroves of the United Arab Emirates.
743 *Journal of Coastal Research* 314, 957–963. [https://doi.org/10.2112/JCOASTRES-D-14-](https://doi.org/10.2112/JCOASTRES-D-14-00142.1)
744 [00142.1](https://doi.org/10.2112/JCOASTRES-D-14-00142.1)

745 Naser, H., Hoad, G., 2011. An investigation of salinity tolerance and salt secretion in
746 protected mangroves, Bahrain. Gulf II: an international conference. The state of the Gulf
747 ecosystem: Functioning and services. Kuwait City, Kuwait. 7-9 February 2011.

748 Ng, W.-T., Rima, P., Einzmann, K., Immitzer, M., Atzberger, C., Eckert, S., 2017.
749 Assessing the Potential of Sentinel-2 and Pléiades Data for the Detection of Prosopis and
750 Vachellia spp. in Kenya. *Remote Sensing* 9, 74. <https://doi.org/10.3390/rs9010074>

751 Pal, M., Mather, P.M., 2005. Support vector machines for classification in remote
752 sensing. *International Journal of Remote Sensing* 26, 1007–1011.
753 <https://doi.org/10.1080/01431160512331314083>

754 Pantaleoni, E., Wynne, R.H., Galbraith, J.M., Campbell, J.B., 2009. Mapping wetlands
755 using ASTER data: a comparison between classification trees and logistic regression.
756 *International Journal of Remote Sensing* 30, 3423–3440.
757 <https://doi.org/10.1080/01431160802562214>

758 Pimple, U., Simonetti, D., Sitthi, A., Pungkul, S., Leadprathom, K., Skupek, H., Som-ard,
759 J., Gond, V., Towprayoon, S., 2018. Google Earth Engine Based Three Decadal Landsat
760 Imagery Analysis for Mapping of Mangrove Forests and Its Surroundings in the Trat
761 Province of Thailand. *Journal of Computer and Communications* 06, 247–264.
762 <https://doi.org/10.4236/jcc.2018.61025>

763 Price, A.R.G., Sheppard, C.R.C., Roberts, C.M., 1993. The Gulf: Its biological setting.
764 *Marine Pollution Bulletin* 27, 9–15. [https://doi.org/10.1016/0025-326X\(93\)90004-4](https://doi.org/10.1016/0025-326X(93)90004-4)

765 Ranjan, A.K., Sivathanu, V., Verma, S.K., Murmu, L., Kumar, P.B.S., 2017. Spatio-
766 temporal variation in Indian part of Sundarban Delta over the years 1990-2016 using
767 Geospatial Technology. *International Journal of Geomatics and Geosciences*. 7. 275-292.

768 Rogers, K., Lymburner, L., Salum, R., Brooke, B.P., Woodroffe, C.D., 2017. Mapping of
769 mangrove extent and zonation using high and low tide composites of Landsat data.
770 *Hydrobiologia* 803, 49–68. <https://doi.org/10.1007/s10750-017-3257-5>

771 Rouse J, Haas R, Schell J, Deering D, editors, 1973. Monitoring vegetation systems in
772 the Great Plains with ERTS. Third ERTS symposium: NASA SP-351. p. 309-317

773 Zhao S., Liu Y., Jiang J., Cheng W., Zhou M., Li M., Ruan R., 2014. Extraction of
774 mangrove in Hainan Dongzhai Harbor based on CART decision tree, in: 2014 22nd

775 International Conference on Geoinformatics. Presented at the 2014 22nd International
776 Conference on Geoinformatics, IEEE, Kaohsiung, Taiwan, pp. 1–6.
777 <https://doi.org/10.1109/GEOINFORMATICS.2014.6950800>

778 Saudi-Aramco, 2016. Saudi Aramco Biodiversity Protection Areas. IPIECA,
779 http://www.ipieca.org/media/2781/saudi_aramco_biodiversity_protection_areas.pdf.

780 Shapiro, A., Trettin, C., Küchly, H., Alavinapanah, S., Bandeira, S., 2015. The
781 Mangroves of the Zambezi Delta: Increase in Extent Observed via Satellite from 1994 to
782 2013. *Remote Sensing* 7, 16504–16518. <https://doi.org/10.3390/rs71215838>

783 Spalding, M., Kainuma, M., Collins, L., 2010. *World atlas of mangroves*

784 Su, Y., Ma, Q., Guo, Q., 2017. Fine-resolution forest tree height estimation across the
785 Sierra Nevada through the integration of spaceborne LiDAR, airborne LiDAR, and
786 optical imagery. *International Journal of Digital Earth* 10, 307–323.
787 <https://doi.org/10.1080/17538947.2016.1227380>

788 Vincini, M., Frazzi, E., D’Alessio, P., 2007. Comparison of narrow-band and broad-band
789 vegetation indexes for canopy chlorophyll density estimation in sugar beet. In:
790 *Proceedings of the 6th European Conference on Precision Agriculture ’07*, Wageningen,
791 The Netherlands, pp. 189–196.

792 Vincini, M., Frazzi, E., D’Alessio, P., 2008. A broad-band leaf chlorophyll vegetation
793 index at the canopy scale. *Precision Agriculture* 9, 303–319.
794 <https://doi.org/10.1007/s11119-008-9075-z>

795 Vo, Q.T., Kuenzer, C., Vo, Q.M., Moder, F., Oppelt, N., 2012. Review of valuation
796 methods for mangrove ecosystem services. *Ecological Indicators* 23, 431–446.
797 <https://doi.org/10.1016/j.ecolind.2012.04.022>

798 Wang, D., Wan, B., Qiu, P., Su, Y., Guo, Q., Wu, X., 2018. Artificial Mangrove Species
799 Mapping Using Pléiades-1: An Evaluation of Pixel-Based and Object-Based
800 Classifications with Selected Machine Learning Algorithms. *Remote Sensing* 10, 294.
801 <https://doi.org/10.3390/rs10020294>

802 Whitney, K., Scudiero, E., El-Askary, H.M., Skaggs, T.H., Allali, M., Corwin, D.L.,
803 2018. Validating the use of MODIS time series for salinity assessment over agricultural

804 soils in California, USA. Ecological Indicators 93, 889–
805 898. <https://doi.org/10.1016/j.ecolind.2018.05.069>

806 Xia, Q., Qin, C.-Z., Li, H., Huang, C., Su, F.-Z., 2018. Mapping Mangrove Forests Based
807 on Multi-Tidal High-Resolution Satellite Imagery. Remote Sensing 10, 1343.
808 <https://doi.org/10.3390/rs10091343>

809